

DATA ASSIMILATION FOR ROBUST UQ WITHIN AGENT-BASED SIMULATION ON HPC SYSTEMS

ADAM SPANNAUS¹, SIFAT AFROJ MOON¹, JOHN GOUNLEY¹, AND HEIDI A. HANSON¹

ABSTRACT. Agent-based simulation provides a powerful tool for *in silico* system modeling. However, these simulations do not provide built-in methods for uncertainty quantification (UQ). Within these types of models a typical approach to UQ is to run multiple realizations of the model then compute aggregate statistics. This approach is limited due to the compute time required for a solution. When faced with an emerging biothreat, public health decisions need to be made quickly and solutions for integrating near real-time data with analytic tools are needed.

We propose an integrated Bayesian UQ framework for agent-based models based on sequential Monte Carlo sampling. Given streaming or static data about the evolution of an emerging pathogen, this Bayesian framework provides a distribution over the parameters governing the spread of a disease through a population. These estimates of the spread of a disease may be provided to public health agencies seeking to abate the spread.

By coupling agent-based simulations with Bayesian modeling in a data assimilation, our proposed framework provides a powerful tool for modeling dynamical systems *in silico*. We propose a method which reduces model error and provides a range of realistic possible outcomes. Moreover, our method addresses two primary limitations of ABMs: the lack of UQ and an inability to assimilate data. Our proposed framework combines the flexibility of an agent-based model with UQ provided by the Bayesian paradigm in a workflow which scales well to HPC systems. We provide algorithmic details and results on a simulated outbreak with both static and streaming data.

1. INTRODUCTION

Infectious disease modeling creates simulations of ongoing or potential disease outbreaks. Assuring accurate estimates for public health agencies seeking input and guidance on the future course of disease is critical during an outbreak. Agent-based modeling (ABM) is a commonly used tool that allows for realistic simulations of disease spread, hospital over-capacity, and mortality when different public health intervention strategies are implemented. While a effective modeling tool, ABMs do not have built-in uncertainty quantification (UQ). The traditional solution is an ensembling approach, which requires running a large number of instances of each simulation and can have large computational costs and delay the time to solution. For example, an agent-based system with millions

Key words and phrases. Mathematics, Statistics, Agent-Based Simulation, Individual-Based Network Epidemic Modeling, Data Assimilation.

This manuscript has been authored by UT-Battelle, LLC under Contract No. DE-AC05-00OR22725 with the U.S. Department of Energy. The United States Government retains and the publisher, by accepting the article for publication, acknowledges that the United States Government retains a non-exclusive, paid-up, irrevocable, worldwide license to publish or reproduce the published form of this manuscript, or allow others to do so, for United States Government purposes. The Department of Energy will provide public access to these results of federally sponsored research in accordance with the DOE Public Access Plan (<http://energy.gov/downloads/doe-public-access-plan>).

of heterogeneous agents requires a significant amount of computational time for just one realization, even in a high-performance computing (HPC) setting [6].

While running multiple simulations to aggregate statistics is a trivially parallel operation, it cannot quantify the parameter estimates of the rates controlling movement between states in an epidemiological model, which are typically specified *a priori*. As the model steps forward in time, it can reflect the range of outcomes conditioned on the parameters governing the ABM simulation itself. Given a shock to the real-world system, such as the emergence of a more virulent strain, the ABM results would fail to reflect this new reality. To sufficiently quantify the new strain’s impact on a population the ABM simulation would require a new set of simulations with different parameters. Moreover, the parameters controlling the movement through the different compartments in an epidemiological model may change with time. For example, treatment regimes may improve as medical professionals have time to study and understand a novel disease, or vaccines may be introduced, reducing the transmissibility of a disease within a proportion of the population. Assimilating real-world data in an online or near-real time fashion would help mitigate some of the shortcomings of ABMs, but these types of models do not have any mechanism to smoothly integrate data, nor a mechanism to update their parameters in response to environmental changes.

The Bayesian paradigm offers solutions to the shortcomings of traditional ABM approaches. By providing distributional information about the disease parameters and the proportion of a population in each of the epidemiological model’s states at each time step, Bayesian methods are a natural way to seamlessly integrate data into a simulation. In particular, sequential Monte Carlo (SMC) methods allow for Bayesian inference within a time series and are widely used in signal tracking, numerical weather prediction, and geophysical applications. This class of methods are widely applicable in inference problems arising in hidden Markov models with possibly noisy and/or partially hidden observations.

There are two limitations with SMC methods which have previously restricted their use. First, this class of methods require a ‘resampling’ step to ensure they capture of the full range of possibilities. This step ensures that the posterior distribution does not degenerate to a point mass and fails to explore the sample space [19]. Moreover, resampling presents a computational bottleneck as it requires a synchronization and reduction step across all processes; the works of [40, 47] seek to lessen this computational burden. Second, designing bespoke proposal distributions allowing for optimal inference in high-dimensional space. In this research, we couple a parallel implementation with limited communication for the resampling scheme to join the individual level fidelity of an ABM with the Bayesian UQ, and defer discussion of the latter to a future work. Figure 1 presents an illustration of our coupling framework.

Our proposed method reduces model error and provides a range of realistic possible outcomes. This work addresses two limitations of ABMs: 1.) an inability to assimilate streaming data into the simulation, accounting for a more virulent strain emerging, improved medical treatments, or inaccessibility of care due to hospital over-capacity; and 2.) the lack of scalable UQ methods. Our method allows for UQ and periodic correction within an ABM, by assimilating real-world data into the solution. Consequently, our proposed method yields results closer to reality as a situation evolves. The codebase is a SMC implementation in Jax, providing an HPC-ready Python package, based in part on [14]. Existing C++ template libraries [51, 32, 52] do not provide a parallel-prefix sum, nor is it available within Python implementations [1, 14]. Additionally, the flexibility of Jax provides performance portability with one codebase on CPUs and GPUs.

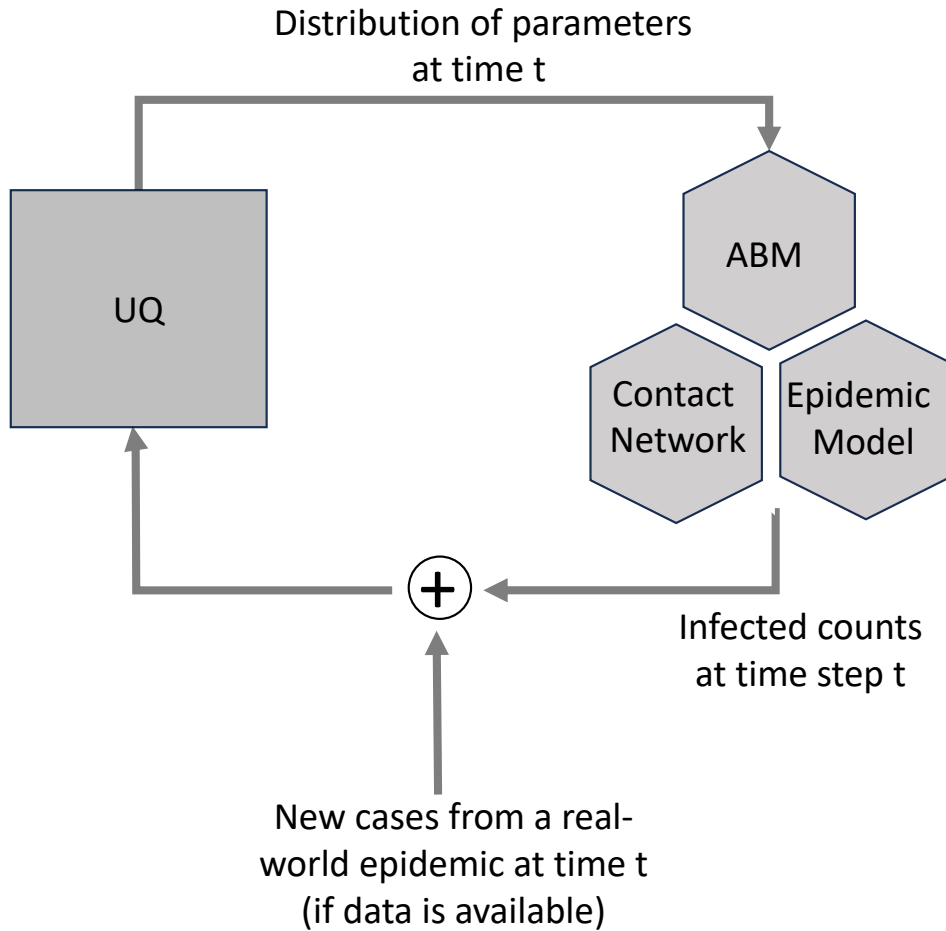


FIGURE 1. Illustration of the coupled ABM and UQ framework. Information is passed between the different methods, yielding high-fidelity ABM simulations and UQ of the model parameters.

1.1. **Related Works.** Other methods have been proposed for incorporating ABMs within a UQ framework, see [4, 15, 28] for example. These proposed solutions are often not effective in a real world scenarios however, due to Gaussian assumptions on the structure of the problem, linearity assumptions on the system dynamics, or numerical approximations within the UQ method itself.

The works of Cocucci et al. and Asher et al. propose two methods to calibrate an ABMs parameters, either through some assumptions on the uncertainties present within the epidemiological model or an approximate Bayesian computation (ABC) framework. Asher et al. [4] describe a (near) real-time dynamic ABM calibration obtained via an ABC setting. Their methodology is applied to a large-scale epidemiological ABM, and had previously only been applied to small toy problems.

Cocucci et al. [15] combine an epidemiological ABM with an ensemble Kalman filter in a data assimilation framework. The Gaussian assumption underlying the Kalman filter

works well if the uncertainties are normally distributed, but the method may fail to capture the disease dynamics in the early or late stages of an outbreak when there are low rates of infection [24]. Moreover, the Monte Carlo approximations of the distributions of interest may fail to converge asymptotically in the case of non-linear dynamics [36], which is the setting of an epidemiological model.

Fadikar et al. present a method that is similar to ours [29]. They employ an importance resampling strategy, but do not address the computational bottlenecks inherent to importance resampling methods. Our previous work [45] and that of Del Moral et al. [20] use SMC coupled with the Particle marginal Markov Chain Monte Carlo methodology [3] to simultaneously infer the epidemiological time-series and governing parameters of the epidemiological model. The primary limitation of these methods is the inability to easily assimilate real-time streaming data into the Markov chain Monte Carlo sampling scheme.

Lastly, the issue of parallel resampling within SMC has been previously addressed by Murray et al. [40], who proposed a few different methods, each with its own set of advantages and limitations. The authors of [31] describe a divide-and-conquer algorithm for efficient resampling within a SMC framework. Our present work uses a CUDA-accelerated implementation of the prefix sum algorithm by Blelloch et al. [8] to compute the cumulative sum over the vector in the high-dimensional weight space in the SMC sampling method.

1.2. Contributions. We describe our approach to provide ABM with scalable Bayesian data assimilation and UQ. Within the data assimilation framework, we connect an ABM model with a Bayesian formulation, integrating data with mathematical models. Data assimilation is a well-established paradigm within the atmospheric and oceanographic modeling communities [36], and gives equal weight to both data and theoretical models. Existing SMC libraries in both Python and C++ do not provide a parallel prefix sum, nor are they easily ported to GPU implementations [51, 32, 52, 1, 14]. Our Jax codebase coupled with the Thrust library provides flexibility for one codebase to run on either a CPU or GPU [11].

In the proof-of-concept experiments considered here, we do not have empirical data. Instead we use a small collection of ABM realizations over a short time window, i.e., a few days to one week, which are used as input to a SMC sampler over the same time span. This sampling method yields distributional estimates of the population proportion in each bin of a compartmental epidemiological model and the parameters governing the rate of movement between those bins. Lastly, any ABM simulation requires the choice of an epidemiological model *a priori*. When faced with an emerging outbreak, sufficient data may not exist to choose one model over another; by framing the problem within the Bayesian framework, model selection based upon the available data is straightforward. One incurs only the additional computational cost of running different simulations in parallel [33].

The outline of the paper is as follows. In Section 2 we give a high-level description of the ABM and SMC methods used. Our algorithmic design is presented in Section 3 and numerical results are in Section 4. We conclude with discussion in Section 5.

2. METHODS

2.1. Epidemiological Modeling. One of the most widely used epidemiological models of disease transmission is the Susceptible-Infected-Removed (SIR) compartmental model [34]. This model describes the movement of a population between three compartments: those who are susceptible to an infection, those who are actively infected, and those who have either recovered from the disease or are deceased due to it. The SIR model has been augmented to include other compartments, such as an exposed individuals, those who have

been exposed but are not actively infected, asymptomatic carriers, or individuals immune to the infection [7]. An ordinary differential equation model of an epidemiological system model assumes population homogeneity and consequently allows for only a small number of variables to describe the system. It tracks the number of individuals in each compartment at each time step. These macro-state variables smooth out the noise in the dynamical system when viewed at the individual level, as through an ABM. The individual-level nature of the ABM drives the stochasticity present within the simulation.

2.1.1. Individual-Based Network Epidemic Modeling. Agent-based modeling is a systematic way to represent heterogeneous, interactive complex systems [26, 46, 5]. It is a useful decision tool in the public health domain to simulate individual-level disease dynamics and agents behaviour. Previous literature has used agent-based simulation to model numerous diseases and complex interventions, such as targeted vaccination, contact tracing, and quarantine strategies [25, 2].

In this work, agents are individual people and connections between them are represented by a social contact network, denoted $G(V, E)$ [44]. We define V as the set of agents and E as the set of undirected edges or links between two agents. A node $v_i \in V$ in G represents an agent. A direct contact between two agents is represented by an edge $e_i \in E$. For the SIR model, agents are divided into each of the three states: susceptible (S), infected (I), and recovered (R). A susceptible agent can contract the disease from an infected agent through direct contact. The transition of an agent from the susceptible to the infected state ($S \rightarrow I$) depends on the health states of its neighboring agents. In contrast, the transition of an agent from the infected to the recovered state ($I \rightarrow R$) does not depend on its neighbors. $H(t)$ keeps track of health state of all agents at time t . The dimension of $H(t)$ is $|V| \times 1$ where $|V|$ is the number of agents and an element of $H(t)$ is denoted $H(t)[v_i] \in \{S, I, R\}$. As a preprocessing step, we divide the agents into multiple MPI (Message Passing Interface) processes. Algorithm 1 outlines the agent-based simulation process for the spread of an SIR model at time t in a single parallel MPI process. After each time step, we synchronize the health state of all agents across all processes.

2.1.2. The Need for Data Assimilation. In ABM, models are defined at the micro scale as a set of values assigned to each agent at some time t . The model defines rules for how these agents interact and how their values evolve with time. For public-health agencies, the specifics of these interactions are not as meaningful as the macro-scale results, e.g., summary statistics of the number of infected individuals or aggregated quantities related to the progression of a disease, such as the percent of hospital capacity in use. While these quantities represent the population as a whole at the macro-level, the goal of the simulation is to faithfully represent the population at the micro-level, but the observations, either from streaming real world data or *in silico* experiments, are not seamlessly integrated into the individual-level simulation. This poses the issue of identifiability, where a bijective mapping between the macro and individual states does not exist. Consequently, we integrate observations into the macro-scale simulations and perform the data assimilation at this level, and will pass the resulting distributional estimates back into the individual-based models, see Figure 1. SMC periodically resamples the ensemble of particles, which are in the epidemiological model’s state space, bypassing the issue of identifiability and the need to adjust the epidemiological compartments in the ABM population at each data assimilation step [15]. Additionally, we chose to discretize the time steps within the SMC simulation at a more granular level than at the ABM simulation, to better identify changing disease trends.

Algorithm 1 Agent-based simulation step at time t for the individual-based network SIR epidemic model in a parallel process.

Input: Network $G(V, E)$;
Set of susceptible nodes at time t in the current process,
 $V_S(t)$;
Set of infected nodes at time t in the current process,
 $V_I(t)$;
Set of recovered nodes at time t in the current process,
 $V_R(t)$;
Health state of nodes at time t , $H(t)$;
Distribution of disease model parameters, $\beta(t)$ and $\gamma(t)$
for SIR compartmental model at time t , and S, I, R compartments.

- 1: New infected nodes $N_I \leftarrow []$
- 2: New recovered nodes $N_R \leftarrow []$
- 3: **for** $v \in V_I(t)$ **do**
- 4: **for** $nbr \in neighbors_of_v$ in G **do**
- 5: **if** $H(t)[nbr] == S$ & nbr is in the same process of v **then**
- 6: $r_1 \leftarrow \mathcal{U}[0, 1]$ // generate a random number
- 7: $r_\beta \leftarrow$ generate a number from the distribution of $\beta(t)$
- 8: **if** $r_1 \leq \frac{r_\beta}{avgD(G)}$ **then** // $avgD(G)$ is the average degree of the contact
network G
- 9: $H(t)[nbr] \leftarrow I$
- 10: $N_I \leftarrow N_I + nbr$
- 11: $V_S(t) \leftarrow V_S(t) - nbr$
- 12: **end if**
- 13: **end if**
- 14: **end for**
- 15: $r_2 \leftarrow \mathcal{U}[0, 1]$ // generate a random number
- 16: $r_\gamma \leftarrow$ generate a number from the distribution of $\gamma(t)$
- 17: **if** $r_2 \leq r_\gamma$ **then**
- 18: $H(t)[v] \leftarrow R$
- 19: $N_R \leftarrow N_R + v$
- 20: $V_I(t) \leftarrow V_I(t) - v$
- 21: **end if**
- 22: **end for**
- 23: $V_I(t) \leftarrow V_I(t) - N_I$
- 24: $V_R(t) \leftarrow V_R(t) - N_R$
- 25: **return** $H(t)$, $V_S(t)$, $V_I(t)$, and $V_R(t)$

2.2. Data Assimilation. Data assimilation is a methodology for probabilistic inference within noisy dynamical systems with partial observations. One of the primary tools for inference in this setting is SMC. Sequential Monte Carlo is a sampling technique used to sequentially analyze a sequence of distributions of a state-space model. Informally, a state-space model relates two discrete or continuous time processes, known as the hidden and observation processes, through a probabilistic model which incorporates densities for both the hidden and observation processes [22]. Traditional sampling methods, such as Markov chain Monte Carlo, struggle with sampling from these high-dimensional distributions due

to correlations between time steps and identifying efficient ways to explore the sample space. SMC methods iteratively generate samples from a sequence of distributions, such as those defined through a dynamical system. These methods are frequently augmented with a data assimilation step, where potentially noisy or sparse observations are incorporated into the algorithm, providing external feedback to the method about some quantities of interest.

Formally, we consider a continuous time Markov process $X_t \in \mathcal{X} \subset \mathbb{R}^d$. For a sequence of times $0 = t_0, \dots, t_n = T$ we will write $y_{1:t} = \{y_\tau\}_{\tau=1}^t$ for a sequence $\{t_i\}_{i=1}^k$ with $k \leq n$ and drop the time subscript for clarity of notation. At time t we are interested in inferring information about some quantity x_t through a possibly indirect observation y_t , which may be corrupted by noise and/or be partially observed. Mathematically this takes the form:

$$(1) \quad X_t \sim p(x_t | x_{t-1}, \theta_x)$$

$$(2) \quad Y_t \sim p(y_t | x_t, \theta_y)$$

for $t \geq 1$, assuming $X_t | X_{t-1}$ and $Y_t | X_t$ admit densities $f(x_t | x_{t-1}; \theta_x)$ and $g(y_t | x_t; \theta_y)$ respectively, for parameters θ_x, θ_y and $X_0 \sim \mu(x_0)$, the prior distribution of x_0 , denoted by μ . Now Equation (1) with the prior μ defines a Bayesian model over the hidden Markov process $\{X_t\}_{t=0}^T$ by considering the posterior parameterized by $\theta := (\theta_x, \theta_y)$ written

$$(3) \quad p_\theta(x_{0:T} | y_{1:T}) = \frac{p_\theta(x_{0:T}, y_{1:T})}{p_\theta(y_{1:T})},$$

which follows from the standard decompositions

$$p_\theta(x_{0:T}, y_{1:T}) = \mu(x_0) \prod_{t=1}^T g(y_t | x_t; \theta_y) \prod_{t=1}^T f(x_t | x_{t-1}; \theta_x)$$

and

$$\begin{aligned} p_\theta(y_{1:T}) &= \prod_{t=1}^T p(y_t | y_{0:t-1}; \theta_y) \\ &= \int_{\mathcal{X}^{T+1}} \mu(x_0) \prod_{t=1}^T g(y_t | x_t; \theta_y) \prod_{t=1}^T f(x_t | x_{t-1}; \theta_x) dx_{0:T}. \end{aligned}$$

If we consider the case of indirect observations, i.e., $Y_t \sim p(y_t | x_t; \theta_y)$ then the goal is to sequentially sample the posterior distribution of the hidden states, i.e., $\{p(x_{0:t} | Y_{1:t} = y_{1:t})\}_{t=1}^T$ in Equation (3), for $1 \leq t \leq T$ and a given set of observations $y_{1:t}$.

In the sequel, a superscript i means for all $i \in \{1, \dots, N\}$ denoting N as the number of particles in an SMC simulation, and a_t^i is the i^{th} element of the ancestor vector A_t where each element in A is the index of the particle at time $t-1$ which is its parent particle at time t . The method proceeds as described in Algorithm 2; the particular algorithmic choices are detailed in Section 4.1.

The choices for reweighting the ensemble on lines 13 and 15 of Algorithm 2 correspond to either the problem of data assimilation or state prediction respectively, depending on the frequency of the observations and problem formulation. We define $q(x_t | x_t^i; \theta_x)$ to be a Gaussian process and let the observation weighting function $r(y_t | x_t^i; \theta_y)$ follow a Gaussian distribution [20, 45]. In this setting, the state transition density $p(x_t | x_{t-1}^i; \theta_x)$ is implicitly defined through a numerical approximation scheme targeting the system Equation (4), but other choices are possible as well. The numerical scheme samples from this transition density, conditioned on the last time step. Other choices are admissible; see [13] for options. In the case that y_t is observed, this choice corresponds to the bootstrap filter [30].

Algorithm 2 Sequential Mote Carlo

```

1: Initialize  $\theta_x, \theta_y$  and sample particles  $\{x_0^i\}_{i=1}^N \sim \mu(x_0)$ 
2: Set  $\{w_0^i\}_{i=1}^N = 1/N$ .
3: for  $t = 1, \dots, T$  do
4:   if resample then
5:      $a_t^i \sim \text{resample}(a_t^{1:N} | w_{t-1}^{1:N})$ 
6:      $w_t^{1:N} \leftarrow 1/N$ 
7:   else
8:      $a_t^i \leftarrow i$ 
9:      $w_t^i \leftarrow w_{t-1}^i / \sum_{j=1}^N w_{t-1}^j$ 
10:  end if
11:   $x_t^i \sim p(x_t | x_{t-1}^{a_t^i}; \theta_x)$  // propagate particles
12:  if  $Y_t$  is observed then // update weights
13:     $w_t^i \leftarrow r(y_t | x_t^i; \theta_y) \cdot w_t^i / w_{t-1}^{a_t^i}$ 
14:  else
15:     $w_t^i \leftarrow q(x_t | x_{t-1}^{a_t^i}; \theta_x) \cdot w_t^i / w_{t-1}^{a_t^i}$ 
16:  end if
17: end for

```

Within the SMC algorithm the resampling step is crucial to its success. Resampling prevents weight degeneracy, where a few particles have non-zero weight, and is triggered by examining the effective sample size of the ensemble [13, 19]. This step is the primary computational bottleneck within the method as it requires a summation across the entire vector $w_t^{1:N}$ of weights when resampling is triggered. There have been some methods proposed to alleviate this bottleneck as described below [40, 31].

2.2.1. Parallel Prefix Resampling. Resampling methods within the SMC literature scale linearly with the number of particles and require a synchronization step, i.e., gathering the entire vector of weights;. These computational considerations have limited the development of SMC methods within an HPC framework. The computational complexity of popular resampling approaches, such as multinomial, residual, systematic, or stratified, increases with the number of particles [40].

We use the Thrust [11] implementation of a parallel prefix-sum algorithm [43] which reduces communication between processes [41], thus addressing the primary computational bottlenecks inherent to the method.

By incorporating a parallel-scan prefix sum, we reduce the computational time to $\mathcal{O}(\log n)$. The prefix sum calculation is a fundamental part of any resampling scheme, as it provides a cumulative sum of the weights, allowing some particles in low-probability regions to die off, while propagating those in regions of higher probability.

In the resampling step, particles are resampled based on their relative importance in the empirical distribution function. Running any SMC, or more generally any sequential importance sampling method, without a resampling step can lead to weight degeneracy problem, especially in the setting of highly-informative observations [13]. Weight degeneracy is where all particles except for one have near-zero weight, leading to a degenerate distribution. Weight degeneracy can be avoided by periodically resampling, which is done by eliminating particles with small weights and replacing them with offspring from those particles that have higher weights, then setting weights for all the particles to be equal.

3. ALGORITHMIC DESIGN

When coupling our ABM simulation with the SMC method we first start from a given set of initial conditions for the ABM. The temporal domain is partitioned into time-steps for the SMC, denoted by τ , and steps where information is passed between the ABM and SMC methods, which are given by t . In our setting, $\tau < t$, as there are some number of steps n which comprise each interval $[t, t + 1]$.

We specify the proportion of the population which is initially infected at the start of the simulation and run the ABM forward in time. The proportion of the population which is in each of the compartments of the epidemiological model at each day are saved as input to the SMC. Other quantities of interest, such as population proportion in the susceptible and recovered compartments, are recorded as well, but are not used by the SMC method.

The SMC sampler then generates a sequence of distributions $\pi_t = \{\pi_\tau\}_{\tau=0}^t$, where $\pi_t = p(x_t | y_{1:t})$ and collection of samples $\{x_\tau\}_{\tau=0}^t$ from the state space. These samples are frequently the proportion of individuals in each compartment of the epidemiological model at time τ . The method may also be defined over an augmented state space and infer time-varying quantities such as disease transmissibility or rate of reporting active cases [23, 45].

At time t we compute summary statistics of the distributional approximations obtained from the SMC method and pass these summaries back to the ABM. As opposed to setting transition rules *a priori* and *post hoc* model aggregation, our iterative process allows for the ABM simulation to better capture the range of possible outcomes. From these updated distributions, we run the ABM simulation forward in time and repeat the process. The pseudo-code for our method is outlined in Algorithm 3.

Algorithm 3 Combined ABM/SMC calibration framework.

Input: $G(V, E)$, n_i (number of infected nodes at $t = 0$)

- 1: Initialize disease model parameters at $t = 0$, $\log \beta_0 \sim \mathcal{U}(-20, 1)$ and $\log \gamma_0 \sim \mathcal{U}(-20, 1)$.
 - 2: Randomly pick a set of infected nodes, $|V_i(t = 0)| = n_i$
 - 3: $H(t = 0)[V_i] = I$
 - 4: $H(t = 0)[V - V_i] = S$
 - 5: **for** $t = 1, \dots, T$ **do**
 - 6: $V_I(t)$ from agent-based simulation (Algorithm 1)
 - 7: Distribution of β_t , and γ_t from SMC (Algorithm 2).
 - 8: **end for**
-

4. NUMERICAL EXPERIMENTS

Experiments are conducted on a GPU-enabled Linux workstation with a NVIDIA RTX A4000 GPU accelerator and CUDA 12.4. The parallel-prefix sum is the Thrust implementation [11]. Our codebase uses Python 3.11 with JAX [10] for the Bayesian modeling and is based on [14]. For the agent-based simulation, we used the Repast library to simulate disease dynamics for an SIR epidemiological model [39, 17]. Single precision computations were used throughout our experiments.

4.1. Epidemiological Modeling Data Assimilation.

4.1.1. *Epidemiological Model.* The epidemiological model used in our SMC experiments is an SIR compartmental model augmented with time-varying transmissibility and recovery rates [20, 45] presented here in Equation (4):

$$(4) \quad \begin{aligned} dS(t) &= -\beta(t)S(t)\frac{I(t)}{N}dt, \\ dI(t) &= (\beta(t)S(t)\frac{I(t)}{N} - \gamma(t)I(t))dt, \\ dR(t) &= \gamma(t)I(t)dt, \\ d \log \beta(t) &= (w_1 - w_2 \log \beta(t))dt + w_3 dB_w(t), \\ d \log \gamma(t) &= (u_1 - u_2 \log \gamma(t))dt + u_3 dB_u(t), \end{aligned}$$

where $\{w_i, u_i\}_{i=1}^3$ parameterize the stochastic differential equations, $d \log \beta$, $d \log \gamma$, and $B_w(t)$, $B_u(t)$ are their respective Brownian motions. The differential equations governing the evolution of β and γ are mean-reverting Ornstein-Uhlenbeck (OU) processes, which allows for some variance within the model output. We choose this stochastic formulation for our experiments to account for the inherent randomness within the ABM simulation and stochastic nature of a disease outbreak.

On the ABM side, we simulated an SIR outbreak of a novel pathogen with transmissibility rate $\beta(t)$, recovery rate $\gamma(t)$, and set the initial infected proportion of the population is 0.2%. For each week in the simulation, we run the ABM, tracking the movement of the population between each compartment within the epidemiological model. The daily counts for each simulated day are collected and only the number of actively infected individuals are sent to the SMC method after one week of simulated time. Then SMC uses these values as observations for an independent simulation of the same week, tracking the proportion of the population in each compartment and inferring the transmissibility and recovery rates. The SMC method computes distributional estimates of the number of individuals within each compartment of the epidemiological model and for $\beta(t)$ and $\gamma(t)$, the latter two values are passed to the ABM for the next week's simulation. This coupling of ABM and SMC obviates the need for thousands of ABM realizations to quantify the uncertainty therein; the Bayesian framework of the SMC method readily computes the necessary estimates.

4.1.2. *Network-Based Simulation Setup.* We use a synthetic social contact network for the ABM simulation. Real-world direct contact networks are often not available in epidemic modeling due to privacy concerns and a lack of individual-level data. Therefore, in our experiments we have generated a contact network which emulates the properties found in real-world networks.

Real-world social contact networks exhibit heavy-tailed degree distribution with community structure [27]. Consequently, we employ a realistic synthetic network, a block two-level Erdős-Rényi (BTER) random network. A BTER network is a well-known graph model that captures observable properties of real-world social networks [44]. A BTER network generator is scalable and can produce a very large network with specific degree distributions and average clustering coefficients. The clustering coefficient of a node v is defined as the probability that neighboring nodes of v in the graph G are also neighbors of each other. A higher average clustering coefficient indicates the presence of well-defined communities or groups in the network.

In this research, we generate a heterogeneous, heavy-tailed BTER network with an average degree of 16.52, consistent with previous social network literature [21]. Eubank et

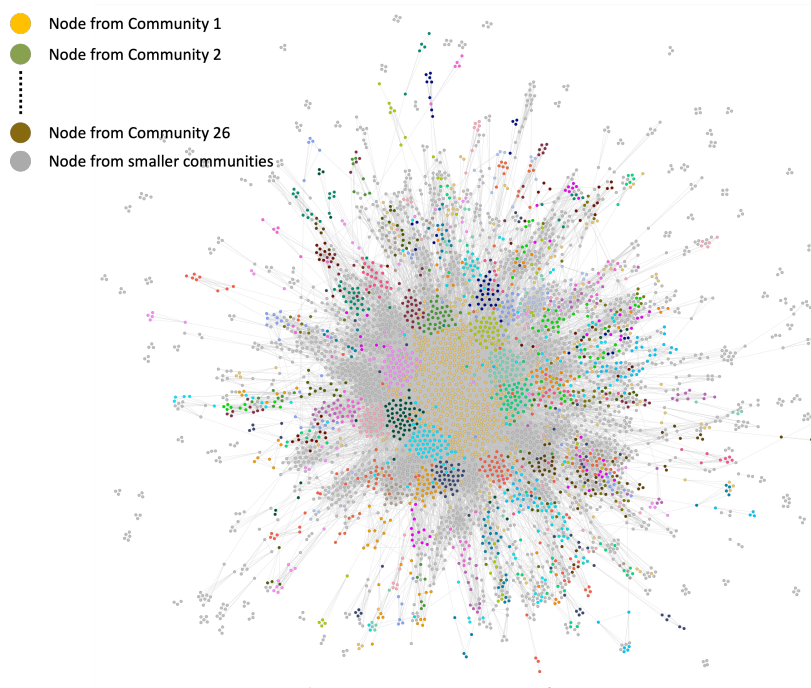


FIGURE 2. A visualization of the generated BTER network containing 5,000 nodes and 415,100 edges. The top 10% largest communities are highlighted with different colors. The gray nodes belong to the smaller communities.

al. [27] have conducted a structural analysis of social contact networks derived from detailed traffic studies, reporting a contact network of 1.6 million individuals in Portland, with a clustering coefficient of around 0.57, which is close to our generated network where the clustering coefficient of the network is approximately 0.55. Network structure affects epidemic prevalence; previous literature finds that a heterogeneous network with community structure is less efficient than a homogeneous network in spreading disease and a high average clustering coefficient is a disadvantage for epidemic spread [38, 50, 49]. Figure 2 shows a visualization of the generated BTER network for this study with 5,000 nodes and 415,100 edges. The dots represent the nodes, and the lines represent the connections between them. The largest connected component in our BTER network contains more than 92% of the nodes. We utilize modularity optimization to detect communities in the network [9]. It detects 268 communities in the BTER network. The top 10% largest communities are highlighted in different colors, with each color representing a distinct community; the gray nodes belong to smaller communities.

We leverage the Repast library, an agent-based simulator, for our network-based epidemic simulation [42, 16]. Repast is a highly scalable distributed modeling framework that spans multiple processing cores via MPI.

4.2. Static Data Assimilation. In our numerical results, we choose $N = 2^{14}$ particles in the SMC method, and set $\beta = 0.5$, $\gamma = 0.1$ for the ABM simulation. This choice of β and γ correspond to a disease with an $R_0 = \beta/\gamma = 5$, similar to what was observed in the

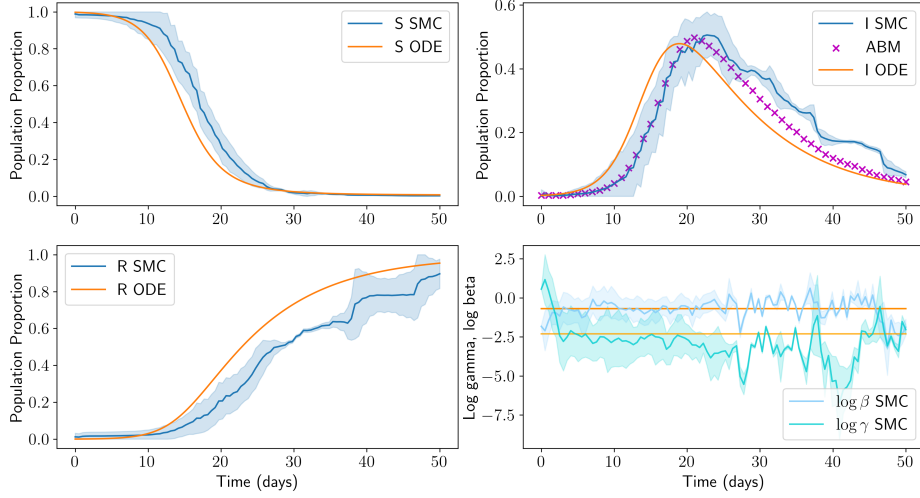


FIGURE 3. Epidemiological curves from an offline ABM calibration, blue lines denote solutions from the SMC, values from the system of epidemiological ordinary differential equations are in orange.

Delta variant of SARS-CoV-2 [37]. These epidemiological parameter values are hidden to the SMC method and are only assigned vague uniform priors. The entire simulation is run for 50 days, with the ABM recording transitions at a daily rate, and passing weekly infected counts to the SMC. The SMC is a bootstrap filter [13] and uses a Gaussian process to interpolate between observations [48]. Designing bespoke proposals which are more informative than the bootstrap proposal are a future direction.

For our first experiment, we consider the setting of offline ABM calibration. We run an ABM simulation with a 4,000 node fully connected network. This setting allows us to directly compare the solution to the system of ordinary differential equations (ODEs) against the output from our coupled ABM/SMC method to see if we can capture behavior that is unavailable to either the ODE system or the ABM alone. To calculate the ABM transmissibility, we find the ratio of $\beta = 0.5$ to the average node degree and set γ as specified above. We saved the ABM output and used the daily infected counts as input to our SMC method. We interpolated one step between each observation, similar to the experimental setup in [20] to ensure stability of our solution. Both started from the same number of infected individuals, but we did not otherwise inform the SMC method. The initial values of β and γ were drawn from vague uniform priors, specifically $\log \beta_0 \sim \mathcal{U}(-20, 1)$, and similarly for $\log \gamma_0$. In the SMC, the population is normalized, so we chose to model the process and observation uncertainty as $\mathcal{N}(0, \sigma^2)$ where $\sigma^2 = 0.1$, representing a 10% error on the state estimation and observations. The results from this simulation are in Figure 3. Our results show that we were able to identify noisy estimates of the transmissibility and recovery rates used in the ABM.

As compared with the values from the static system of ODEs we closely followed the ODE curve. Our method was able to identify the overall trajectory after the initial uncertainty, reducing the width of the 95/5% credible intervals as the simulation time progressed. Although our method was able to identify the trajectory of the recovered class, we observe greater uncertainty in these estimates, as the credible intervals are wider here,

when compared with those in the susceptible class. This is due to the uncertainty in our estimates of β and γ , which control movement into and out of the infected compartment.

Turning now to the initial two weeks of the infected proportion, we observe a trajectory which under-estimates the infected proportion as compared to the ODE solution, and has wide credible intervals towards the peak of the infected curve, indicating greater uncertainty in the distributional estimates at those times. Focusing on a time window starting after the two week mark, in Figure 4 we have plotted the kernel density estimates of these distributions to understand the source of this greater uncertainty. In this sequence of plots, we observe that the distributions start multimodal, with the estimated density quite diffuse. These densities have a greater spread than those at the end of this subset of time, due to the wide credible intervals for γ .

As time progresses, we see that these density estimates become more concentrated and have a distinct peak by the end of this window. This initial multi-modality is driven by the wide intervals about β and γ for the first half of the simulation window. While the value of γ decreases for the first few time steps and identifies the general neighborhood of γ , we observe wider credible intervals here, as compared with the latter half of the simulation, leading to the greater uncertainty in the infected curve for the first half. Additionally, this leads to a somewhat later infected peak time, but also more importantly, a greater proportion of the population being infected. This greater infected peak is driven in part by the under-estimation of γ , this extending the recovery period.

This increased variance and large moves in the γ curve are reflected in the wide credible intervals for the recovered compartment after day 40 in the simulation. While both the infected and recovered curve follow the trend in the ODE solution, the jumps in γ are reflected in the credible intervals about the recovered proportion due to the structure of the differential equations.

To further decrease the width of the credible intervals for this setting we may choose different observational densities, or by calibrating with real data, so that the value of γ used in the ABM is closer to real-world conditions. Since the ABM does not assume population homogeneity unlike the ODE, increasing the variance of the estimated quantities might better capture the dynamics driving recovery.

We observe that the inferred values of the infected curve lag somewhat, but not dramatically so, behind those from the ODE system, this is due in part to the delayed infectivity seen in the ABM. The values of γ towards the end of the simulation directly impacts the number of infected individuals, which sets up the discrepancy between the inferred and ODE curves. One potential strategy to mitigate this disagreement, is to use a larger ensemble of particles within the SMC method, i.e., increase N , or another is to increase the variance, w_3 , within the stochastic differential equation, $d \log \beta(t)$ in Equation (4).

Lastly, we examine the inferred densities from 100 ABM simulations to see if our proposed method can capture behavior which is not seen by aggregating ABM simulations. In Figure 5 we have the infected curves from 100 ABM simulations with the same experimental setup as above and the kernel density estimates (KDEs) over the same timespan as Figure 4. Comparing the KDEs between our coupled method and aggregated simulations, we can see how our model is able to capture the uncertainty and multimodality present in the system for this timespan. The aggregated ABM cannot adapt since both the transmissibility and recovery rates were set *a priori*. Also note that the infected curve from the ABM lags behind the ODE solution, as seen in Figure 3. Since the ODE system is the continuous-time asymptotic limit as the ABM timestep decreases to 0 for a fully connected

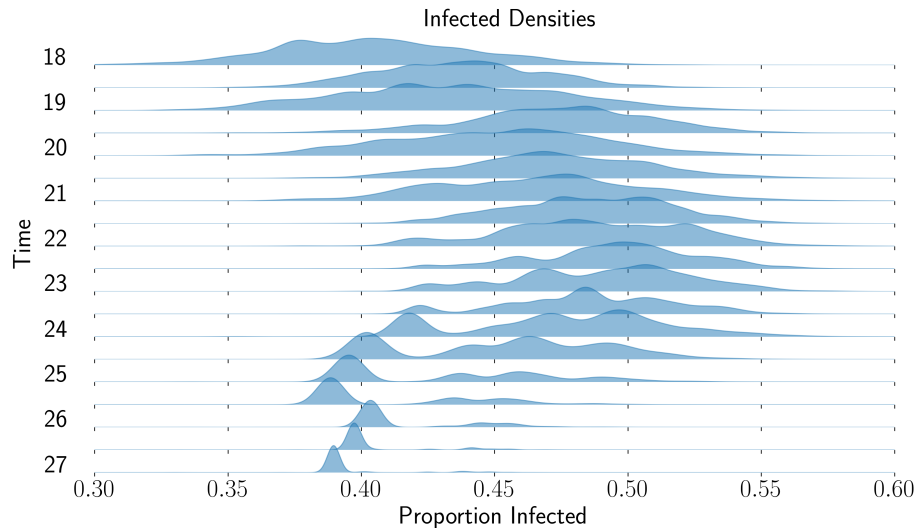
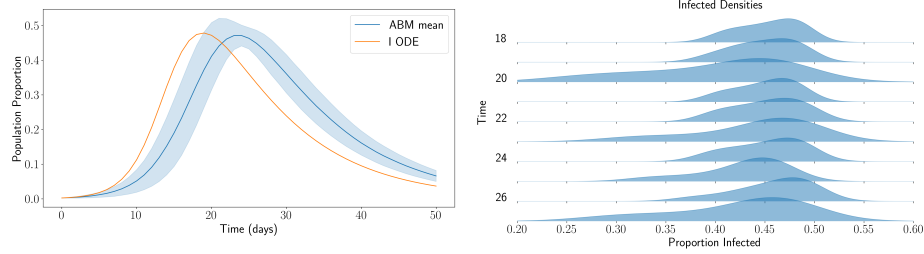


FIGURE 4. Infected curves from an offline ABM calibration from a subset of the entire time window; density curves were estimated through a kernel density estimate. Notice the multi-modality of the inferred distributions at the beginning of the time window, which concentrate as the simulation progresses.



(A) Infected curves from 100 ABM simulations (B) Kernel density estimates from 100 ABM simulations and ODE solution.

FIGURE 5. In fig (a) we see infected curves from 100 ABM simulations and their corresponding kernel density estimates in (b). Notice while the resulting density estimates are not Gaussian, they do not exhibit the multi-modality seen in Figure 4.

network, the choice of ABM timestep of one day limits the number of possible interactions that agents may have, causing this delay in infections.

4.3. Streaming Data Assimilation. For our second experiment, we dynamically integrate observational data from our ABM into our SMC method. Specifically, we randomly initialize the values of β and γ from vague uniform priors for both the ABM and SMC, as in our previous experiments, and start both simulations from the same number of infected individuals. After one week of ABM simulation time, we pass the number of infected

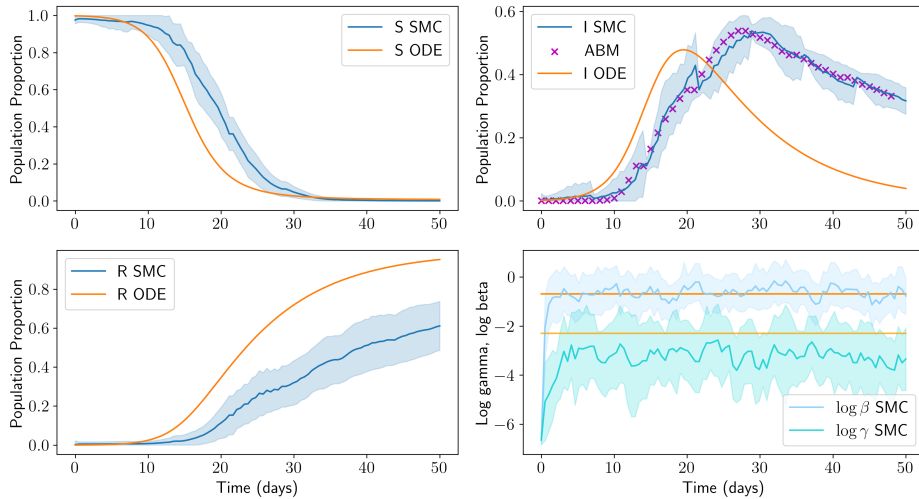


FIGURE 6. Epidemiological curves from an on-line ABM calibration, blue lines denote average solutions from the SMC distributions; values from the system of epidemiological ordinary differential equations are in orange, and ABM values are denoted by purple markers. Shaded regions denote 95% credible intervals about the mean.

individuals at each day to the SMC as observations. We then run the SMC forward for the same duration. At the end of this interval, we compute distributional estimates of β and γ and pass these estimates back to the ABM for the next time window. The epidemiological curves from this experiment are presented in Figure 6.

For this experiment we compare the results from our coupled ABM and SMC method with the solution of the system of ODEs with constant values of β and γ , corresponding to Equation (4) the setting where $d \log(\beta(t)) = d \log(\gamma(t)) = 0$ for $0 \leq t \leq T$. When comparing the results in Figure 6 from our simulation against the ODE solution we observe generally good agreement between the mean inferred value of the susceptible class for the duration of the simulation. We observe that the recovered class is underestimated for approximately half of the simulation time, due to the difference between the ODE solution and inferred values for the infected class and the slower rate of recovery, i.e., lower value of γ . This discrepancy in the infected curve can be seen from the infected proportion, especially for the latter half of the simulation time. While the inferred infected curve initially lags behind that from the ODE solution, a greater proportion of the population is infected in the coupled ABM/SMC simulation as compared with the static ODE solution. This difference is driven by the value of $\gamma(t)$ which effecting the infected class in two ways: 1.) it exhibits greater variability than does $\beta(t)$ and 2.) is generally lower than the constant value for the simulation.

When comparing the differences in the infected class for the first half of the simulation window, one can see that the ABM underestimates the proportion of infections, due in part to the initial estimate of β . The initial value significantly underestimated the transmissibility of the disease, estimating that for every 10,000 persons fewer than 1 would become infected, when the ‘true’ transmissibility rate would yield 5,000 infections. While the inferred value of β was able to identify the ODE value within the first few simulation days, the decreased

proportion of individuals becoming infected contributed in part to the difference between the peak infection times in the coupled ABM/SMC simulation and the ODE solution.

Examining the inferred values for β and γ , we broadly see two trends: 1.) the inferred $\beta(t)$ was able to recover from the poor initialization and identify the constant value used in the ODE solution; and 2.) the inferred γ shows greater variability and wider credible intervals as compared with β , both due to the uncertainty in the infected class.

The infected class occupies a unique position within our epidemiological model. From a modeling perspective, it is dependent on each of the other compartments and model parameters; from a public health viewpoint, knowing its peak value and range of possible outcomes allows public health agencies to plan for various scenarios, assessing hospital capacity and consider if intervention strategies are needed. Examining this curve for the first three simulation weeks, we observe that follows a similar trend to that of the ODE solution, albeit delayed. A greater proportion of the population is infected in the coupled simulation, due in part to the increased recovery time, i.e., decreased value of γ , and uncertainty in its estimates.

5. DISCUSSION

We have developed a data assimilation method which augments the state-space of a partially observed dynamical system with an ABM. This framework allows for more realistic epidemiological modeling of a population, as classical ODE methods assume population homogeneity. Coupling these two approaches yields a tool capable of quantifying: 1.) the spread of a disease in a heterogeneous population, and 2.) the possible range of outcomes by assimilating near-real time streaming data into the model. While the proof-of-concept runs conducted in this study are moderately sized, the SMC-based approach and associated packages like Repast scale well and should be suitable for deployment on HPC systems.

Our results demonstrate the efficacy of this approach in settings with either static or streaming data. There are a few directions which would further improve our modeling strategy. It is widely known within the SMC community that identifying good proposal distributions, i.e., the pushforward measure of the ensemble from t to $t + 1$, is challenging. This issue is magnified in the present setting, where we have specified the functional form of the time-varying components *a priori* in Equation (4). The formulation employed here assumes some steady-state, where $\log \beta$ and $\log \gamma$ are in some interval about their mean. This scenario may not always be realistic however. If we consider the setting of a viral mutation or the emergence of a drug resistant strain, the mean-reverting Ornstein–Uhlenbeck processes modeled here would no longer be applicable. Rather, either of these scenarios would require formulating a new epidemiological model and performing new simulations, thus increasing the time before public health agencies can act. One possible solution to this limitation would be to learn the functional form of the dynamics from the data itself, instead of specifying it. This is precisely the goal of neural differential equations [12, 35].

Another direction which would improve our model’s inferences is to generate the distributional estimates for the time-varying parameters from the smoothing distribution as opposed to the filtering distribution within the SMC model. These two distributions are related [36], but provide different information. The filtering distribution provides $\pi(x_t | y_t)$ whereas the smoothing distribution considers the entire observation trajectory $\pi(x_t | y_{1:t})$, which ‘smoothes’ out the roughness introduced by the noise in the pushforward measure when going from t to $t + 1$. This increased path regularity comes at a computational cost, as typical algorithms scale linearly in time. A recent work [18] reduces the computational

cost to $O(\log_2 T)$ through a clever combination step when stitching together the resulting posterior distributions.

5.1. Conclusions. Our proposed data assimilation method successfully combines the power of a micro-scale epidemiological simulation within a Bayesian framework to quantify the uncertainty and make model corrections at each time-step. Our data assimilation framework allows for integrating near-real time data into an ABM, keeping the results closer to reality as a situation evolves. Our framework also allows for time-varying parameters to be seamlessly included into the underlying epidemiological model. We rule out implausible parameter choices within the ABM, thus reducing model error and providing a range of realistic outcomes.

The resulting epidemiological curves from our static and streaming data experiments demonstrate that our framework captures the time-varying dynamics of a disease outbreak and adapts the model to the dynamics within the data. By calibrating our ABM with real-world data, the inferred epidemiological parameters will be closer to reality than the standard ABM modeling setup, as the latter approach cannot dynamically react to changes in epidemiological structure. Solutions to a system of epidemiological ODEs also fail to capture the entirety of the system at the necessary fidelity, due to their reliance on the assumption of population homogeneity. It is through coupling these two strategies within a Bayesian framework that we may provide a method to assimilate near-real time data into ABM simulations to advise public health agencies faced with a novel disease outbreak.

ACKNOWLEDGMENTS

This manuscript has been authored by UT-Battelle, LLC, under contract DE-AC05-00OR22725 with the US Department of Energy (DOE). The US government retains and the publisher, by accepting the article for publication, acknowledges that the US government retains a nonexclusive, paid-up, irrevocable, worldwide license to publish or reproduce the published form of this manuscript, or allow others to do so, for US government purposes. DOE will provide public access to these results of federally sponsored research in accordance with the DOE Public Access Plan (<http://energy.gov/downloads/doe-public-access-plan>).

DECLARATIONS

Funding. This material is based upon work supported by the U.S. Department of Energy, Office of Science, Office of Advanced Scientific Computing under Award Number DE-SC-ERKJ422.

Availability of data and materials. The code used to create the figures and simulation results are in a git repository:

<https://github.com/aspannaus/abm-uq>.

Competing interests. The authors declare that they have no competing interests.

REFERENCES

- [1] ABRIL-PLA, O., ANDREANI, V., CARROLL, C., DONG, L., FONNESBECK, C. J., KOCHUROV, M., KUMAR, R., LAO, J., LUHMANN, C. C., MARTIN, O. A., OSTHEGE, M., VIEIRA, R., WIECKI, T., AND ZINKOV, R. PyMC: a modern, and comprehensive probabilistic programming framework in Python. *PeerJ Comput. Sci.* 9 (Sept. 2023).
- [2] AFROJ MOON, S., MARATHE, A., AND VULLIKANTI, A. Are all underimmunized measles clusters equally critical? *Royal Society Open Science* 10, 8 (2023), 230873.

- [3] ANDRIEU, C., DOUCET, A., AND HOLENSTEIN, R. Particle markov chain monte carlo methods. *Journal of the Royal Statistical Society: Series B (Statistical Methodology)* 72, 3 (2010), 269–342.
- [4] ASHER, M., LOMAX, N., MORRISSEY, K., SPOONER, F., AND MALLESON, N. Dynamic calibration with approximate bayesian computation for a microsimulation of disease spread. *Scientific Reports* 13, 1 (2023), 8637.
- [5] BARRETT, C. L., BISSET, K. R., EUBANK, S. G., FENG, X., AND MARATHE, M. V. Episimdemics: an efficient algorithm for simulating the spread of infectious disease over large realistic social networks. In *SC'08: Proceedings of the 2008 ACM/IEEE Conference on Supercomputing* (2008), IEEE, pp. 1–12.
- [6] BHATTACHARYA, P., MACHI, D., CHEN, J., HOOPS, S., LEWIS, B., MORTVEIT, H., VENKATRAMANAN, S., WILSON, M. L., MARATHE, A., POREBSKI, P., ET AL. Novel multi-cluster workflow system to support real-time hpc-enabled epidemic science: Investigating the impact of vaccine acceptance on covid-19 spread. *Journal of Parallel and Distributed Computing* 191 (2024), 104899.
- [7] BLACKWOOD, J. C., AND CHILDS, L. M. An introduction to compartmental modeling for the budding infectious disease modeler. *Letters in Biomathematics* 5, 1 (2018), 195–221.
- [8] BLELLOCH, G. E. Prefix sums and their applications.
- [9] BLONDEL, V. D., GUILLAUME, J.-L., LAMBIOTTE, R., AND LEFEBVRE, E. Fast unfolding of communities in large networks. *Journal of statistical mechanics: theory and experiment* 2008, 10 (2008), P10008.
- [10] BRADBURY, J., FROSTIG, R., HAWKINS, P., JOHNSON, M. J., LEARY, C., MACLAURIN, D., NECULA, G., PASZKE, A., VANDERPLAS, J., WANDERMAN-MILNE, S., AND ZHANG, Q. JAX: composable transformations of Python+NumPy programs, 2018.
- [11] CCCL DEVELOPMENT TEAM. CCCL: CUDA C++ Core Libraries, 2023.
- [12] CHEN, R. T., RUBANOVA, Y., BETTENCOURT, J., AND DUVENAUD, D. K. Neural ordinary differential equations. *Advances in neural information processing systems* 31 (2018).
- [13] CHOPIN, N., PAPASPILIOPOULOS, O., ET AL. *An introduction to sequential Monte Carlo*, vol. 4. Springer, 2020.
- [14] CHOPIN, N., PAPASPILIOPOULOS, O., ET AL. *Particles*, 2023.
- [15] COCUCCI, T. J., PULIDO, M., APARICIO, J. P., RUIZ, J., SIMOY, M. I., AND ROSA, S. Inference in epidemiological agent-based models using ensemble-based data assimilation. *Plos one* 17, 3 (2022), e0264892.
- [16] COLLIER, N., AND OZIK, J. Distributed agent-based simulation with repast4py. In *2022 Winter Simulation Conference (WSC)* (2022), IEEE, pp. 192–206.
- [17] COLLIER, N. T., OZIK, J., AND TATARA, E. R. Experiences in developing a distributed agent-based modeling toolkit with python. In *2020 IEEE/ACM 9th Workshop on Python for High-Performance and Scientific Computing (PyHPC)* (2020), IEEE, pp. 1–12.
- [18] CORENFLOS, A., CHOPIN, N., AND SÄRKKÄ, S. De-sequentialized monte carlo: a parallel-in-time particle smoother. *Journal of Machine Learning Research* 23, 283 (2022), 1–39.
- [19] DEL MORAL, P., DOUCET, A., AND JASRA, A. Sequential monte carlo samplers. *Journal of the Royal Statistical Society: Series B (Statistical Methodology)* 68, 3 (2006), 411–436.
- [20] DEL MORAL, P., AND MURRAY, L. M. Sequential monte carlo with highly informative observations. *SIAM/ASA Journal on Uncertainty Quantification* 3, 1 (2015), 969–997.
- [21] DEL VALLE, S. Y., HYMAN, J. M., HETHCOTE, H. W., AND EUBANK, S. G. Mixing patterns between age groups in social networks. *Social Networks* 29, 4 (2007), 539–554.
- [22] DOUCET, A., DE FREITAS, N., GORDON, N. J., ET AL. *Sequential Monte Carlo methods in practice*, vol. 1. Springer, 2001.
- [23] DUREAU, J., KALOGEROPOULOS, K., AND BAGUELIN, M. Capturing the time-varying drivers of an epidemic using stochastic dynamical systems. *Biostatistics* 14, 3 (2013), 541–555.
- [24] EBEIGBE, D., BERRY, T., SCHIFF, S. J., AND SAUER, T. Poisson kalman filter for disease surveillance. *Physical Review Research* 2, 4 (2020), 043028.
- [25] ESPINOZA, B., ADIGA, A., VENKATRAMANAN, S., WARREN, A. S., CHEN, J., LEWIS, B. L., VULLIKANTI, A., SWARUP, S., MOON, S., BARRETT, C. L., ET AL. Coupled models of genomic surveillance and evolving pandemics with applications for timely public health interventions. *Proceedings of the National Academy of Sciences* 120, 48 (2023), e2305227120.
- [26] EUBANK, S., GUCLU, H., ANIL KUMAR, V., MARATHE, M. V., SRINIVASAN, A., TOROCZKAI, Z., AND WANG, N. Modelling disease outbreaks in realistic urban social networks. *Nature* 429, 6988 (2004), 180–184.
- [27] EUBANK, S., KUMAR, V. A., MARATHE, M. V., SRINIVASAN, A., AND WANG, N. Structure of social contact networks and their impact on epidemics. *DIMACS Series in Discrete Mathematics and Theoretical Computer Science* 70 (2006), 181.
- [28] FADIKAR, A., STEVENS, A., COLLIER, N., TOH, K. B., MOROZOVA, O., HOTTON, A., CLARK, J., HIGDON, D., AND OZIK, J. Towards improved uncertainty quantification of stochastic epidemic models using sequential monte carlo, 2024.

- [29] FADIKAR, A., STEVENS, A., COLLIER, N., TOH, K. B., MOROZOVA, O., HOTTON, A., CLARK, J., HIGDON, D., AND OZIK, J. Towards improved uncertainty quantification of stochastic epidemic models using sequential monte carlo. *arXiv preprint arXiv:2402.15619* (2024).
- [30] GORDON, N. J., SALMOND, D. J., AND SMITH, A. F. Novel approach to nonlinear/non-gaussian bayesian state estimation. In *IEE proceedings F (radar and signal processing)* (1993), vol. 140, IET, pp. 107–113.
- [31] GULDAS, H., CEMGIL, A. T., WHITELEY, N., AND HEINE, K. A practical introduction to butterfly and adaptive resampling in sequential monte carlo. *IFAC-PapersOnLine* 48, 28 (2015), 787–792.
- [32] JOHANSEN, A. M. Smctc: sequential monte carlo in c++. *Journal of Statistical Software* 30 (2009), 1–41.
- [33] KASS, R. E., AND RAFTERY, A. E. Bayes factors. *Journal of the american statistical association* 90, 430 (1995), 773–795.
- [34] KERMACK, W. O., AND MCKENDRICK, A. G. A contribution to the mathematical theory of epidemics. *Proceedings of the royal society of london. Series A, Containing papers of a mathematical and physical character* 115, 772 (1927), 700–721.
- [35] KIDGER, P. On neural differential equations. *arXiv preprint arXiv:2202.02435* (2022).
- [36] LAW, K., STUART, A., AND ZYGALAKIS, K. Data assimilation. *Cham, Switzerland: Springer* 214 (2015), 52.
- [37] LIU, Y., AND ROCKLÖV, J. The reproductive number of the delta variant of sars-cov-2 is far higher compared to the ancestral sars-cov-2 virus. *Journal of travel medicine* 28, 7 (2021), taab124.
- [38] LIU, Z., LAI, Y.-C., AND YE, N. Propagation and immunization of infection on general networks with both homogeneous and heterogeneous components. *Physical Review E* 67, 3 (2003), 031911.
- [39] MACAL, C. M., COLLIER, N. T., OZIK, J., TATARA, E. R., AND MURPHY, J. T. Chisim: An agent-based simulation model of social interactions in a large urban area. In *2018 winter simulation conference (WSC)* (2018), IEEE, pp. 810–820.
- [40] MURRAY, L. M., LEE, A., AND JACOB, P. E. Parallel resampling in the particle filter. *Journal of Computational and Graphical Statistics* 25, 3 (2016), 789–805.
- [41] NICELY, M. A., AND WELLS, B. E. Improved parallel resampling methods for particle filtering. *IEEE Access* 7 (2019), 47593–47604.
- [42] OZIK, J., WOZNIAK, J. M., COLLIER, N., MACAL, C. M., AND BINOIS, M. A population data-driven workflow for covid-19 modeling and learning. *The International Journal of High Performance Computing Applications* 35, 5 (2021), 483–499.
- [43] SÄRKKÄ, S., AND GARCÍA-FERNÁNDEZ, Á. F. Temporal parallelization of bayesian smoothers. *IEEE Transactions on Automatic Control* 66, 1 (2020), 299–306.
- [44] SESHADHRI, C., KOLDA, T. G., AND PINAR, A. Community structure and scale-free collections of erdős-rényi graphs. *Physical Review E—Statistical, Nonlinear, and Soft Matter Physics* 85, 5 (2012), 056109.
- [45] SPANNAUS, A., PAPAMARKOU, T., ERWIN, S., AND CHRISTIAN, J. B. Inferring the spread of covid-19: the role of time-varying reporting rate in epidemiological modelling. *Scientific reports* 12, 1 (2022), 10761.
- [46] TOROCZKAI, Z., AND EUBANK, S. *Agent-based modeling as a decision-making tool*. National Academies Press: Washington, DC, USA, 2005.
- [47] WHITELEY, N., LEE, A., AND HEINE, K. On the role of interaction in sequential monte carlo algorithms.
- [48] WILLIAMS, C. K., AND RASMUSSEN, C. E. *Gaussian processes for machine learning*, vol. 2. MIT press Cambridge, MA, 2006.
- [49] WU, X., AND LIU, Z. How community structure influences epidemic spread in social networks. *Physica A: Statistical Mechanics and its Applications* 387, 2-3 (2008), 623–630.
- [50] ZANETTE, D. H. Dynamics of rumor propagation on small-world networks. *Physical review E* 65, 4 (2002), 041908.
- [51] ZHOU, Y. vsmc: parallel sequential monte carlo in c++. *Journal of Statistical Software* 62 (2015), 1–49.
- [52] ZHOU, Y. Monte carlo kernel library. <https://github.com/zhouyan/MCKL/tree/master>, 2018.

Email address, Corresponding author: spannausat@ornl.gov

(1) OAK RIDGE NATIONAL LABORATORY, OAK RIDGE, TN 37830